Carbohydrate Polymers 118 (2015) 150–155

Contents lists available at ScienceDirect

Carbohydrate Polymers

journal homepage: www.elsevier.com/locate/carbpol

Crystalline characteristics of cellulose fiber and film regenerated from ionic liquid solution

Liangfeng Sun [a], Jonathan Y. Chen [a,*], Wei Jiang [a], Vincent Lynch [b]

[a] School of Human Ecology, The University of Texas at Austin, Austin, TX 78712, USA
[b] Department of Chemistry, The University of Texas at Austin, Austin, TX 78712, USA

ARTICLE INFO

Article history:
Received 6 December 2013
Received in revised form 25 October 2014
Accepted 10 November 2014
Available online 15 November 2014

Keywords:
Regenerated cellulose
Fiber
Film
Ionic liquid
X-ray diffraction
Crystallinity

ABSTRACT

Regenerated cellulose fiber, fiber extrudate, and film were produced from cellulose solution prepared with raw pulp and ionic liquid solvent 1-butyl-3-methylimidazolium chloride ([BMIM]Cl). Spinning setting was based on a dry-jet and wet-spun approach including extrusion, coagulation, drawing, drying, and winding. Crystallization of the experimental fiber, fiber extrudate, and film was evaluated using a technique of wide angle X-ray diffraction (WAXD). Crystallinity index, crystallite size, and crystal orientation factor were calculated and compared among these samples. Influence of die shape, die dimension, and drawing speed on the regenerated cellulose crystallinity was discussed. The study indicated that the pulp cellulose was a Cellulose I type structure. The cellulose regeneration from the [BMIM]Cl solution completed a transformation from this intermediate phase to a final Cellulose II phase. The die shape and dimension and drawing speed were all important factors affecting the crystallinity of regenerated cellulose fiber and film.

1. Introduction

Current rayon production capacity accounts for approximately 5% of the world man-made fiber production. It is predicted that global rayon production and demand will grow at an increasing rate of 3.8% per year from 2009 to 2014 (Blagoev, Bizzari, & Inoguchi, 2011). Although rayon fiber is still a major regenerated cellulose fiber commercially available for many end uses, its manufacturing approach is making a significant environment impact because of heavy use of strong acids and bases and high consumption of water and energy. Recent cellulose research has paid much attention to ionic liquids that can be ideal green solvents for dissolving raw cellulose in the production of regenerated cellulose fiber (Gutowski et al., 2003; Hesse-Ertelt, Heinze, Kosan, Schwikal, & Meister, 2010; Kosan, Dorn, Meister, & Heinze, 2010a; Rogers, Holbrey, Spear, & Swatloski, 2002; Swatloski, Holbrey, Weston, & Rogers, 2006; Swatloski, Spear, Holbrey, & Rogers, 2002; Wang, Gurau, & Rogers, 2012). Ionic liquids are a type of organic salts having a liquid phase below boiling temperature. Their cationic component determines chemical stability, while their anionic part plays an important role in chemical reaction (Fukaya, Sugimoto, & Ohno, 2006; Greaves & Drummond, 2013; Hu et al., 2013; Kosan, Michels, & Meister, 2008; Wang, Gurau, Kelley, Myerson, & Rogers, 2013). Compared to the widely used rayon technology and Tencel®/Lyocell® technology (Fink, Weigel, & Purz, 2001; Hayhurst & Banks, 2005; Kosan, Dorn, & Meister, 2010; Liu & Hu, 2006; Wendler, Graneß, Büttner, Mechtler, & Heinze, 2006; Wendler, Graneß, & Heinze, 2005), it is found that the use of ionic liquids for making cellulose solutions renders several advantages such as lower dissolving temperature (below 100 °C) and vapor pressure, lower to zero toxicity, better thermal stability, no hydrolysis, and easy solvent recovery (Hermanutz, Gaehr, Uerdingen, Meister, & Kosan, 2008; Zhao et al., 2012; Zhu et al., 2006). These technical attractions drive a lot of research investigation.

Fabrication of regenerated cellulose fiber using the ionic liquid solvent 1-butyl-3-methyllimidazolium chloride ([BMIM]Cl) was first reported in Michels and Kosan's (2005) work. They found that a transformation of cellulose I to cellulose II occurred after [BMIM]Cl dissolution and cellulose precipitation in water bath, as previously observed in lyocell spinning that uses *N*-methylmorpholine-*N*-oxide monohydrate (NMMO) for cellulose dissolution. This result was also mentioned in the work of Cai, Zhang, Guo, Shao, and Hu (2010). Similar work on using [BMIM]Cl to dissolve bagasse cellulose for fiber spinning was reported (Jiang, Sun, Hao, & Chen, 2011). Regenerated cellulose fiber was also produced from cellulose solutions prepared by the ionic liquids 1-ethyl-3-methylimidazolium acetate ([EMIM]Ac) and 1-ethyl-3-methylimidazolium diethyl phosphates ([EMIM]DEP) (Ingildeev,

* Corresponding author. Tel.: +1 512 471 0633; fax: +1 512 471 5630.
E-mail address: jychen2@austin.utexas.edu (J.Y. Chen).

http://dx.doi.org/10.1016/j.carbpol.2014.11.008
0144-8617/

Effenberger, Bredereck, & Hermanutz, 2013), for a comparison with the cellulose fiber regenerated from NMMO solution. Kosan et al. conducted a comparative study on the four ionic liquids, [BMIM]Cl, 1-*N*-butyl-3-methylimidazolium acetate ([BMIM]Ac), 1-ethyl-3-methylimidazolium chloride ([EMIM]Cl), and [EMIM]Ac, for the dissolution and regeneration of cellulose (Kosan et al., 2008). In a study reported recently, [EMIM]Ac solvent was applied to the preparation of cellulose solution mixed with polysaccharide particles (Wendler et al., 2010).

Overall, the research efforts mentioned above were focused mainly on solute solubility, solution viscosity, fiber spinning process, fiber tensile strength, and fiber crystallinity. To deal with ionic liquids, understanding how they work for dissolving cellulose polymer would be critical to both researchers and fiber manufacturers. Further research is needed to continue the investigation on ionic liquids in terms of their efficiency for cellulose dissolution, mechanism of cellulose crystallization during fiber coagulation, and processability for cellulose fiber spinning, so that the rayon industry would be able to produce regenerated cellulose fiber using ionic liquids as an eco-friendly new solvent system. This paper presents a study on the materials of regenerated cellulose fiber and film fabricated from a [BMIM]Cl solution. A major purpose of this work was to examine influences of spinning conditions on cellulose crystallization taken place during fiber/film precipitation in water bath.

2. Materials and methods

2.1. Solution preparation and fiber/film spinning

Raw materials used in the study were commercial grade southern pine pulp with a DP of 1900 and [BMIM]Cl solvent (purity > 95%) purchased from Sigma-Aldrich Corp., USA. The fabrication of regenerated cellulose fiber/film involved two steps: dissolution of cellulose in [BMIM]Cl to make spinning dope and extrusion of the spinning dope to form regenerated cellulose fiber and film. Experimental procedure used in this study was the same as that described in the previous publication (Jiang et al., 2011). In brief, the cellulose solution with 6 wt% cellulose concentrations was prepared by adding ground wood pulp into [BMIM]Cl solvent for dissolving under controlled heating and vacuuming. The obtained cellulose solution was fed into a desk-top screwless extruder for extruding the solution into a water bath where cellulose fiber/film was precipitated when the ionic liquid was washed away by tap water. Rotor speed of the extruder was controlled within 169 – 221 rpm. Spin header was heated to 100 °C for spinning with a 30-mm air gap above the spin bath. Regenerated cellulose fiber was drawn at a spin-draw ratio between 10 and 30, dried when passing through a tube with 80–100 °C hot air flow, and finally wound onto a spool using a winding device with a winding speed ranging from 80 to 225 mm/s. The experimental fiber ran a second-time washing and drying under the same dry setting.

2.2. Characterization of fiber/film crystallinity

To investigate the degree of crystallinity, crystal size, and crystallite orientation of the regenerated cellulose fiber and film, the technique of wide angle X-ray diffraction (WAXD) was used. X-ray diffraction patterns of pulp board, cellulose fiber, and film were measured by the WAXD instrument RAPID II (Rigaku Americas Corporation). The instrument has a curved imaging plate area detector which is able to collect the complete Debye rings of samples measured in transmission. A bundle of cellulose fibers were mounted vertically on the gonimeter. During measurements, the fiber sample rotated at a constant speed of one degree per second. Since fiber samples were mounted vertically and rotated constantly (or rotationally symmetric), the φ setting has little effect on the diffraction patterns. For pulp board and cellulose film, a strip of sample cut along the machine direction was mounted vertically on the gonimeter. The position of sample was fixed with a surface perpendicular to the X-ray direction during measurement. All the tests lasted for 90 min. Blank tests were run under the same conditions as fiber and film X-ray diffraction. The 2-D images of blank tests were removed from the 2-D images of fiber and film X-ray diffraction to reduce the effect of background diffraction. The meridional reflections of fiber have a maximum intensity at the Bragg angle. Based on the amount of the meridional reflection, which have a maximum intensity, different percent crystallinities of cellulose samples would be determined. The experimental X-ray diffraction patterns were simulated by the following mathematical model (Ruland, 1961; Vonk, 1973; Hindeleh & Johnson, 1974; Jing, Zhang, & Wu, 2002):

$$Y = \sum_{i=1}^{n} Q_i + R \tag{1}$$

where

$$Q_i = f_i G_i + (1 - f_i) C_i$$

$$R = a + bx + cx^2 + dx^3$$

In the above equations, Y is the total diffraction intensity of all crystalline and non-crystalline parts; Q_i is individual diffraction intensity from each crystal part; G_i and C_i are Gaussian and Lorentz functions, respectively; f_i is a fractional parameter; n is the number of total diffraction peaks; R is the intensity of amorphous halo from non-crystalline part; and a, b, c, and d are four constants. All the parameters in the model above were determined using a least squares regression method (curve fitting) which was implemented by the MATLAB curve fitting program. The parameters for crystalline peaks of Cellulose I and II were used as the initial input parameters of the model in Eq. (1).

The fiber/film crystallinity index (CI) could be calculated by a ratio between sum of area under each crystalline peak and area under the experimental diffraction curve:

$$CI = \frac{\text{sum of area under each crustalline peak } (Q_i)}{\text{area under experimental diffraction curve}} \tag{2}$$

In this analysis of crystallinity index, an assumption was made that the amorphous contribution is the only contribution to the X-ray diffraction peak broadening. Other factors such as crystallite size which might contribute to the peak broadening were not considered a contributor to the diffraction peak broadening (Garvey, Parker, & Simon, 2005).

The cellulose uniaxial crystallite orientation along fiber axis is determined by the Herman's crystal orientation factor f_c defined as:

$$f_c = 1 - \frac{3}{2}\left(\frac{\int_0^{\pi/2} I(\varphi)\sin^3\varphi d\varphi}{\int_0^{\pi/2} I(\varphi)\sin\varphi d\varphi}\right) \tag{3}$$

where $I(\varphi)$ is intensity of scattered diffraction and φ is azimuthal angle (Krassig, 1996). For cellulose film, a biaxial orientation factors should be used. It was reported that the crystalline orientation of polymer films is closely related to that in the polymer fibers. We would only calculate the uniaxial orientation factor of fibers in this study.

The crystallite size L is calculated by the Scherrer equation:

$$L = \frac{k\lambda}{\beta \cos\theta} \tag{4}$$

where k is a geometrical Scherrer constant ($k = 0.94$); λ is the X-ray wave length (for Cu radiation $\lambda = 1.54$ Å); β is the intensity of full

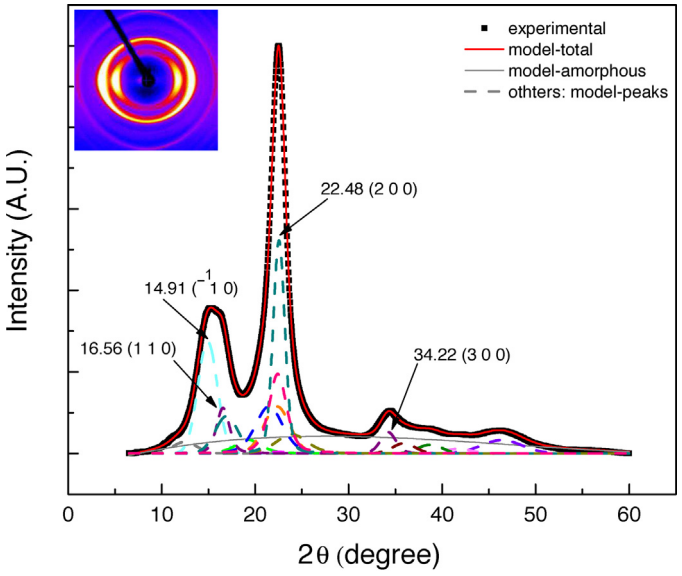

Fig. 1. WAXD diffraction pattern, profile, and calculated crystal peaks of raw pulp.

width at half maximum (FWHM); and θ is the Bragg angle (Guérin & Alvarez, 1995).

3. Results and discussion

3.1. Morphology and crystal polymorphic structure of pulp cellulose and regenerated cellulose

WAXD patterns of 2D images in the insert and 1D integrated X-ray diffraction intensity profiles of the pulp cellulose and regenerated cellulose are given in Figs. 1 and 2. Pulp board showed rings of diffraction pattern and cellulose fiber showed the spots of diffraction patterns. The big difference between the diffraction profiles of pulp board and cellulose fiber is that the highest diffraction peak shifted to a lower Bragg angle for the cellulose fiber. Since X-ray scattering from amorphous region produces a halo image and that from a crystalline region produces strong rings or spots, the integrated intensity profiles from amorphous X-ray images have a very

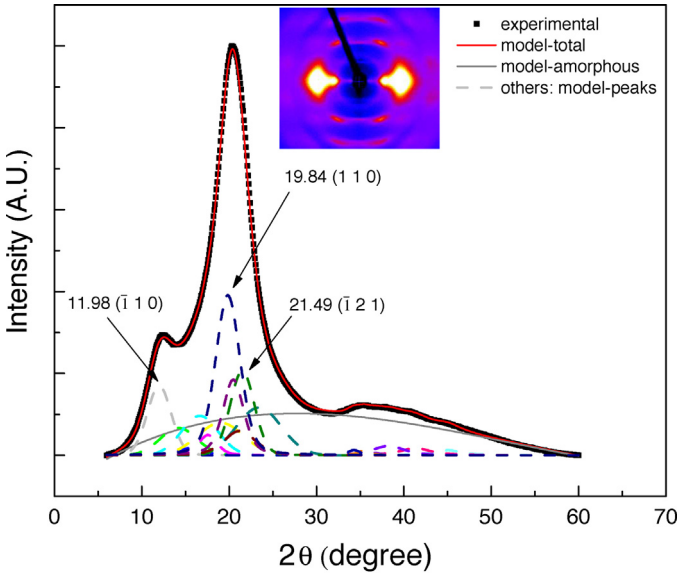

Fig. 2. WAXD diffraction pattern, profile, and calculated crystal peaks of pure regenerated cellulose fiber.

broad, low intensity curve and that from crystalline region have a sharp, high intensity peaks. In order to estimate the crystallinity index from the X-ray diffraction patterns, the one-dimensional total scattering spectrum is deconvoluted into amorphous and crystalline scattering parts. The cellulose crystalline regions are indicated by calculated diffraction peaks (Q_i) and the cellulose amorphous regions are determined by a calculated halo curve (R). As references to the phase diagrams of Celluloses I and II, the phases and reflection angles were calculated by the freeware Chekcell, assuming that Cellulose I has unit cell dimensions of $a = 7.906$ Å, $b = 8.201$ Å, $c = 10.38$ Å, $\alpha = 90°$, $\beta = 90°$, and $\gamma = 96.5°$ and Cellulose II has unit cell dimensions of $a = 8.10$ Å, $b = 9.03$ Å, $c = 10.31$ Å, $\alpha = 90°$, $\beta = 90°$, and $\gamma = 117.10°$ (Wada, Nishiyama, Chanzy, Forsyth, & Langan, 2008). The curve-fitting process yields 16 crystalline peaks and one amorphous halo for the pulp sample, as seen in Fig. 1. Out of the 16 peaks, four crystalline peaks ($\bar{1}$ 1 0, 1 1 0, 2 0 0 and 3 0 0) from Cellulose I have been assumed or reported in other studies (Park, Baker, Himmel, Parilla, & Johnson, 2010; He, Cui, & Wang, 2008; Cheng, Varanasi, & Li, 2011).

From Fig. 1, it could be observed that the pulp cellulose diffraction profile was very similar to the cellulose I diffraction profile (Wada, Kondo, & Okano, 2003; Garvey et al., 2005; Cheng et al., 2011). The main peak at position 22.48° was a typical peak for cellulose I. The separated two broad peaks at positions 14.91° and 16.56° were close to the difftaction peaks from cellulose I (14.9° and 16.7° for I_β; 14.3° and 16.8° for I_α). The forth peak at 34.22° was close to the small diffraction peak at 34.5° from cellulose I. Referred to Fig. 2, the crystalline structure of the regenerated cellulose was typically a cellulose II crystalline structure and was illustrated by three Cellulose II peaks located at $2\theta = 11.98°$ ($\bar{1}$ 1 0), 19.84° (1 1 0), and 21.49 ($\bar{1}$ 2 1) (Ago, Endo, & Hirotsu, 2004; Hori & Wada, 2006; Kumar, Gupta, Lee, & Gupta, 2010), plus a very weak Cellulose I peak at $2\theta = 34.28$ (3 0 0). The three diffraction peaks from cellulose I, as discussed above in pulp cellulose, were gone in the diffraction profile of regenerated cellulose fiber. This means that Cellulose II became a dominant structure in pure regenerated cellulose. Thus, the WAXD data verifies the fact that through the process of using BMIMCl to dissolve and regenerate cellulose, the structure of the pulp cellulose experienced a transformation from its initial phase in which Cellulose I and II co-existed to its terminated phase in which Cellulose II dominated. This result was consistent with that reported in previous research (Berger, Keck, & Philipp, 1988; O'Sullivan, 1997; Michels & Kosan, 2005). It was also noticed that the regenerated cellulose had an enhanced halo curve, meaning that the amorphous regions increased in the regenerated cellulose.

3.2. Effect of die shape and dimension

Calculated crystalline characteristics of the regenerated cellulose extruded from different die shapes are listed in Table 1. It could be seen that the crystallinity of the regenerated cellulose was significantly affected by the die shapes. The crystalline structure of the raw cellulose pulp featured a highest crystallinity index (72.2%) and largest crystallite size (2.946 nm). In contrast to this, the regenerated cellulose fiber samples Fiber 1 and Fiber 2 indicated lower crystallinity indexes, smaller crystallite sizes, and higher crystal orientation. Please note that the average crystallite size from all peaks is smaller, but the calculated crystallite size from only phase (2 0 0) of cellulose pulp is 5.72 nm, which is in the range of 4 to 7 nm in most references (He et al., 2008; Cao & Tan, 2005). The c-axis orientation factors for Fibers 1 and 2 are 0.377 and 0.455, respectively. These lower orientation factors may be due to the low draw ratio of the fiber and higher cellulose chain flexibility. By examining Fibers 1 and 2, it could also be observed that a reduction of die diameter did not cause a significant change in fiber crystallinity, but resulted in an increase in crystallite size and crystal orientation factor. The

Table 1
Crystallinity index, crystal size, and orientation factor of regenerated cellulose fiber, extrudate, and film produced from 6% cellulose solution with different spinning conditions (values in parentheses are standard deviation).

Sample	Type of die	Drawing speed (mm/s)	Crystallinity index (%)	Crystallite size (nm)	Orientation factor
Fiber 1	1/8″ tube die	80	67.2 (±0.2)	1.946 (±0.002)	0.377 (±0.005)
Fiber 2	1/16″ filament die	80	67.0 (±0.1)	1.985 (±0.004)	0.455 (±0.003)
Extrudate	1/16″ filament die	0	60.4 (±0.3)	1.905 (±0.005)	0.219 (±0.000)
Film	3/4″-wide film die	0	48.5 (±0.3)	2.057 (±0.004)	–
Raw pulp	N/A	N/A	72.2	2.946	–

sample Extrudate was cellulose fiber spun in the spin bath without any drawing. It is not difficult to understand that it had a lower crystallinity index, lower crystallite size, and much lower crystal orientation compared to Fibers 1 and 2.

The cellulose film was extruded with a film die of 3/4″ width. It was held by a transfer roll with water rinse before it entered into water bath for precipitation without drawing. Because of this spinning approach, it could be expected that the film crystallinity index and orientation factor were all lower than those of Fibers 1 and 2 and Extrudate. However, it was interestingly observed that the crystallite size of Film was higher than that of Fibers 1 and 2 and Extrudate. A possible reason for this might be from the film extrusion method mentioned above and from the fact that the produced film was thinner. The use of the transfer roll and water rinse not only imposed a certain drawing action on the cellulose solution but also caused an earlier solution quench. This would promote cellulose nucleation and crystal growth which might be controlled by a diffusion process. For a visual comparison, Fig. 3 exhibits the WAXD diffraction profiles of regenerated cellulose film, extrudate, and fiber produced from [BMIM]Cl solution with an addition of 1 wt% silver nanoparticle. The short pulse-like peaks on the diffraction curves reflects the silver crystals. Obviously, the regenerated cellulose fiber indicates the highest crystallinity, followed by the regenerated cellulose extrudate and film.

The orientation of crystalline regions in the regenerated cellulose could also be evaluated by the azimuthal reflection profile. The zero degree of azimuthal angel means that the crystalline aligns in the longitudinal direction of the fiber. The 90° of azimuthal angel indicates that the crystalline aligns in the transverse direction of the fiber. Therefore, for a flatter curve of the diffraction profiles, a lower orientation factor is expected. The fiber having a steeper curve of the diffraction profiles implies a higher crystalline orientation factor. Fig. 4 plots the $I(\varphi)$–φ curves of the regenerated cellulose samples Fiber II, Extrudate, and Film. Using Fiber II as a reference, the crystal orientation along fiber/film longitudinal direction was visually compared among these samples, with Fiber II representing the highest degree of crystal orientation, and with Film exhibiting the least crystal orientation.

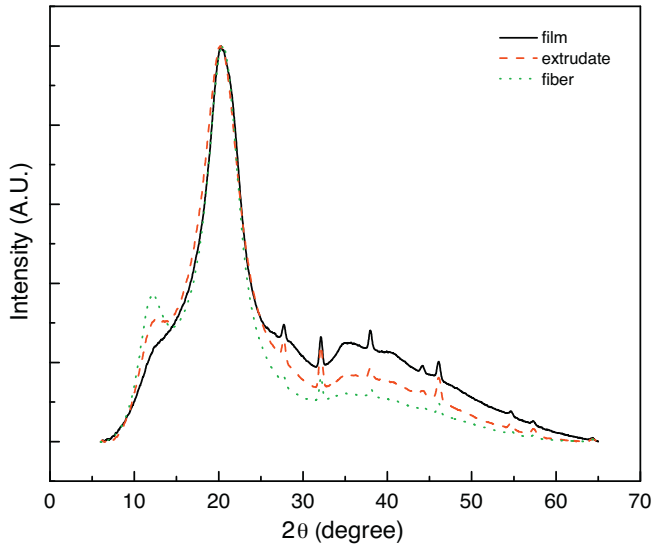

Fig. 3. Comparison of WAXD diffraction profiles of regenerated cellulose film, extrudate, and fiber (with 1 wt% nanosilver filler).

3.3. Drawing speed effect

Crystallinity of the regenerated cellulose fiber spun in different drawing speeds was evaluated based on the WAXD data. Table 2 lists calculated results. Clearly, the increase of fiber drawing speed helped increase the cellulose crystalline region, crystal growth, and alignment of the crystalline region along fiber axial direction. When the cellulose solution prepared from [BMIM]Cl was extruded into the water bath, fiber precipitation occurred through solution quenching and antisolvent (water) addition into the solution system. An addition of the antisolvent reduced the solubility of cellulose in [BMIM]Cl, resulting in a condition of supersaturation that was a driving force for cellulose nucleation and growth. Because a new solid cellulose phase could be created by nucleation from the supersaturated solution phase, the condition of supersaturation

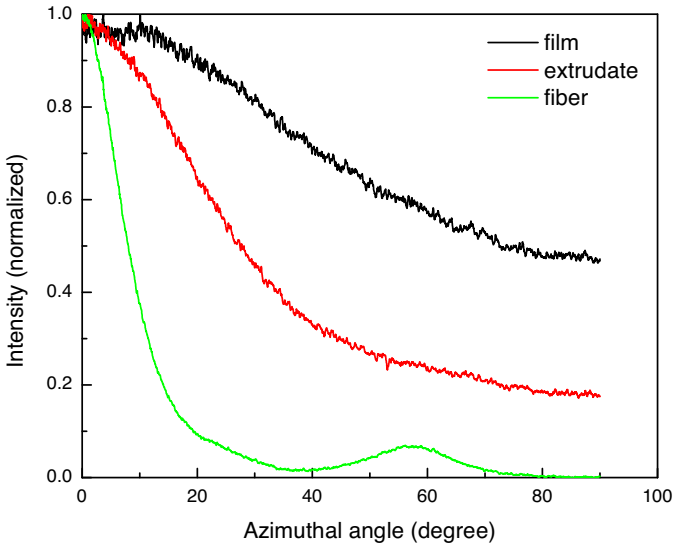

Fig. 4. Comparison of azimuthal reflection profile of regenerated cellulose film, extrudate, and fiber.

Table 2
Crystalline characteristics of the regenerated cellulose fiber spun with 6 wt% cellulose solution and a tube die.

Line speed (m/s)	Crystallinity index (%)	Crystallite size (nm)	Orientation factor
0.080	67.2 (±0.2)	1.946 (±0.002)	0.377 (±0.005)
0.165	67.7 (±0.3)	1.956 (±0.002)	0.404 (±0.002)
0.252	68.7 (±0.1)	1.963 (±0.003)	0.426 (±0.000)
0.296	69.0 (±0.1)	1.966 (±0.005)	0.461 (±0.016)

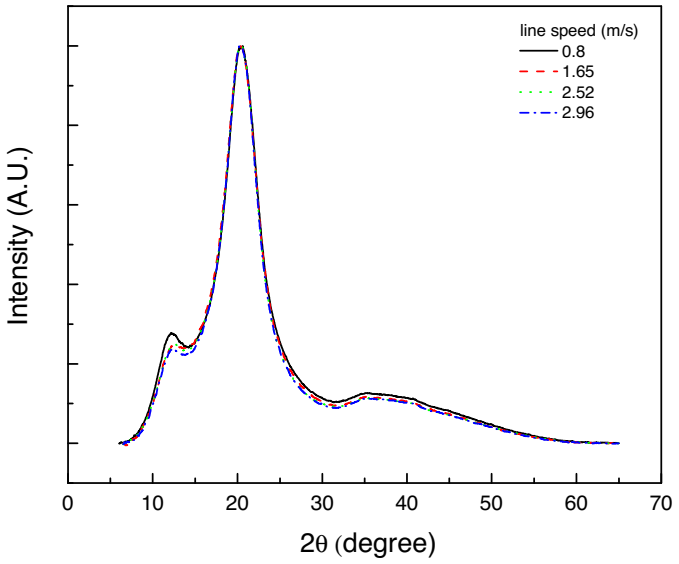

Fig. 5. WAXD diffraction profiles of the regenerated cellulose fiber prepared with different drawing speeds.

became critical for the precipitation process of the regenerated cellulose fiber. When the regenerated cellulose fiber was subject to an increasing drawing during the spinning, its lateral dimension (diameter) was reduced in the water bath, causing a larger fiber surface area and reducing the barrier of surface diffusion of the antisolvent. As a result, the cellulose solution in precipitation reached a high supersaturation that accelerated the nucleation and crystal growth.

Fig. 5 plots the WAXD diffraction profiles of the regenerated cellulose fiber spun with the 4 drawing speeds. The significant differences were observed in the 2θ range between 12° and 20° where the fiber produced with the highest drawing speed indicated the strongest Cellulose II crystallinity, while the fiber drawn at the lowest speed revealed the lowest Cellulose II crystallinity. The azimuthal reflection profiles for these fiber samples are plotted in Fig. 6, indicating the cellulose crystal orientation along the fiber longitudinal direction. As expected, the regenerated cellulose fiber spun with the highest drawing speed had the highest degree

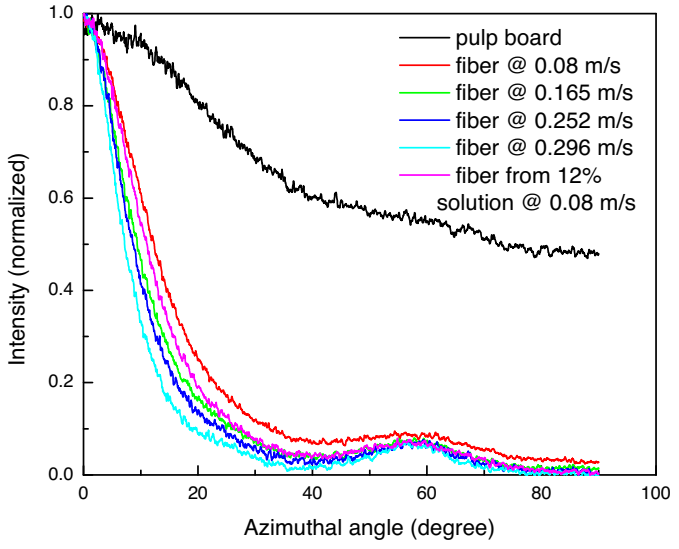

Fig. 6. Comparison of azimuthal reflection profiles between the raw pulp and cellulose fiber spun with different drawing speeds.

of crystal orientation. Fig. 6 also includes a cellulose fiber extruded with a [BMIM]Cl solution of 12 wt% of cellulose concentration and drawn at the lowest speed of 80 mm/s. The crystal orientation of this fiber was just slightly higher than that of the cellulose fiber produced with 6 wt% cellulose solution and drawing speed of 80 mm/s. This revealed that the fiber drawing speed was a main effect to improve fiber crystal orientation. The increase of cellulose concentration in the solution alone did not help very much for increasing the cellulose fiber crystal orientation.

4. Conclusions

The pulp cellulose used in this study showed a polymorphous Cellulose I type structure. After the dissolution using [BMIM]Cl and cellulose regeneration during the fiber spinning, the Cellulose I polymorphous structure was transformed into the Cellulose II structure almost completely. Die shape and dimension of the spinning head affected the regenerated cellulose crystallinity. The regenerated cellulose film indicated the lowest crystallinity index and crystal orientation factor compared to the regenerated cellulose fiber. But the film crystal size was significantly higher than that of the fiber probably because of the film initial drawing imposed by a film deposit roll. It was confirmed that the smaller-diameter die helped increase cellulose crystallinity, crystal size, and crystal orientation under the same drawing speed. The spinning drawing speed was also proven a main effect influencing the crystallinity of the regenerated cellulose fiber. The higher the drawing speed, the higher are the values of fiber crystallinity index, crystal size, and orientation factor.

Acknowledgment

The authors are grateful for the use of Rigaku Rapid II R-Axis Spider Diffractometer purchased through the The National Science Foundation (NSF) support funds (NSF Grant No. 0741973).

References

Ago, M., Endo, T., & Hirotsu, T. (2004). Crystalline transformation of native cellulose from cellulose I to cellulose ID polymorph by a ball-milling method with a specific amount of water. *Cellulose*, *11*, 163–167.

Berger, W., Keck, M., & Philipp, B. (1988). On the mechanism of cellulose dissolution in non-aqueous solvents, especially in O-basic systems. *Cellulose Chemistry and Technology*, *22*, 387–397.

Blagoev, M., Bizzari, S., & Inoguchi, Y. (2011). *Rayon and lyocell fibers*. IHS Chemical. Retrieved 2-4-2011, from ⟨http://www.sriconsulting.com/CEH/Public/Reports/541.3000/⟩.

Cai, T., Zhang, H. H., Guo, Q. H., Shao, H. L., & Hu, X. C. (2010). Structure and properties of cellulose fibers from ionic liquids. *Journal of Applied Polymer Science*, *115*, 1047–1053.

Cao, Y., & Tan, H. (2005). Study on crystal structures of enzyme-hydrolyzed cellulosic materials by X-ray diffraction. *Enzyme Microbial Technology*, *36*, 314–317.

Cheng, G., Varanasi, P., Li, C., et al. (2011). Transition of cellulose crystalline structure and surface morphology of biomass as a function of ionic liquid pretreatment and its relation to enzymatic hydrolysis. *Biomacromolecules*, *12*(4), 933–941.

Fink, H. P., Weigel, P., & Purz, H. J. (2001). Structure formation of regenerated cellulose materials from NMMO-solutions. *Progress in Polymer Science*, *26*, 1473–1524.

Fukaya, Y., Sugimoto, A., & Ohno, H. (2006). Superior solubility of polysaccharides in low viscosity, polar, and halogen-free 1,3-dialkylimidazolium formates. *Biomacromolecules*, *7*, 3295–3297.

Garvey, C. J., Parker, I. H., & Simon, G. P. (2005). On the interpretation of X-ray diffraction powder patterns in terms of the nanostructure of cellulose I fibres. *Macromolecular Chemistry and Physics*, *206*, 1568–1575.

Greaves, T. L., & Drummond, C. J. (2013). Solvent nanostructure, the solvophobic effect and amphiphile self-assembly in ionic liquids. *Chemical Society Reviews*, *42*, 1096–1120.

Guérin, D. M. A., & Alvarez, A. G. (1995). A survey on the determination of crystal size in powder diffractometry. *Crystallography Reviews*, *4*, 261–277.

Gutowski, K. E., Broker, G. A., Willauer, H. D., Huddleston, J. G., Swatloski, R. P., Holbrey, J. D., et al. (2003). Controlling the aqueous miscibility of ionic liquids: Aqueous biphasic systems of water–miscible ionic liquids and water-structuring salts for recycle, metathesis, and separations. *Journal of the American Chemical Society*, *125*, 6632–6633.

Hayhurst, M. J., & Banks, A. J. (2005). Observations on Lyocell fiber formation. *Lenzinger Berichte*, *84*, 103–109.
He, J., Cui, S., & Wang, S.-Y. (2008). Preparation and crystalline analysis of high-grade bamboo dissolving pulp for cellulose acetate. *Journal of Applied Polymer Science*, *107*, 1029–1038.
Hermanutz, F., Gaehr, F., Uerdingen, E., Meister, F., & Kosan, B. (2008). New developments in dissolving and processing of cellulose in ionic liquids. *Macromolecular Symposia*, *262*, 23–27.
Hesse-Ertelt, S., Heinze, T., Kosan, B., Schwikal, K., & Meister, F. (2010). Solvent effects on the NMR chemical shifts of imidazolium-based ionic liquids and cellulose therein. *Macromolecular Symposia*, *294-II*, 75–89.
Hindeleh, A. M., & Johnson, D. J. (1974). Crystallinity and crystallite size measurement in cellulose fibres: 2. Viscose rayon. *Polymer*, *15*, 697–705.
Hori, R., & Wada, M. (2006). The thermal expansion of cellulose II and III crystals. *Cellulose*, *13*, 281–290.
Hu, X. M., Xiao, Y. B., Niu, K., Zhao, Y., Zhang, B. X., & Hu, B. Z. (2013). Functional ionic liquids for hydrolysis of lignocellulose. *Carbohydrate Polymers*, *97*, 172–176.
Ingildeev, D., Effenberger, F., Bredereck, K., & Hermanutz, F. (2013). Comparison of direct solvents for regenerated cellulosic fibers via the lyocell process and by means of ionic liquids. *Journal of Applied Polymer Science*, *128*, 4141–4150.
Jiang, W., Sun, L., Hao, A., & Chen, J. Y. (2011). Regenerated cellulose fibers from waste bagasse using ionic liquid. *Textile Research Journal*, *81*, 1949–1958.
Jing, A. J., Zhang, A., & Wu, Z. (2002). Thermal analysis of polymer fibers in handbook of thermal analysis and calorimetry: Vol. 3. In Stephen Z. D. Cheng, & Patrick K. Gallagher (Eds.), *Applications to polymers and plastics* (pp. 409–482). Amsterdam: Elsevier (Chapter 11).
Kosan, B., Dorn, S., Meister, F., & Heinze, T. (2010). Preparation and subsequent shaping of cellulose acetates using ionic liquids. *Macromolecular Materials and Engineering*, *295*, 676–681.
Kosan, B., Michels, C., & Meister, F. (2008). Dissolution and forming of cellulose with ionic liquids. *Cellulose*, *15*, 59–66.
Kosan, B., Schwikal, K., & Mechtler, K. (2010). Solution states of cellulose in selected direct dissolution agents. *Cellulose*, *17*, 495–506.
Krassig, H. A. (1996). Cellulose-structure, accessibility and reactivity. In M. B. Huglin (Ed.), *Polymer monographys*. Amsterdam, The Netherlands: Gordon and Breach Science Publishers.
Kumar, S., Gupta, R., Lee, Y. Y., & Gupta, R. B. (2010). Cellulose pretreatment in subcritical water: Effect of temperature on molecular structure and enzymatic reactivity. *Bioresource Technology*, *101*, 1337–1347.
Liu, R., & Hu, X. (2006). Precipitation kinetics of cellulose in the lyocell spinning process. *Industrial and Engineering Chemistry Research*, *45*, 2840–2844.
Michels, C., & Kosan, B. (2005). Contribution to the dissolution state of cellulose and cellulose derivatives. *Lenzinger Berichte*, *84*, 62–70.
O'Sullivan, A. C. (1997). Cellulose: The structure slowly unravels. *Cellulose*, *4*, 173–207.
Park, S., Baker, J. O., Himmel, M., Parilla, P. A., & Johnson, D. K. (2010). Cellulose crystallinity index: Measurement techniques and their impact on interpreting cellulase performance. *Biotechnology for Biofuels*, *3*(10), 1–10.
Rogers, R. D., Holbrey, J. D., Spear, S. K., & Swatloski, R. P. (2002). Ionic liquids: A look at the dissolution of cellulose. In *6th annual green chemistry and engineering conference* (pp. 39–40).
Ruland, W. (1961). X-ray determination of crystallinity and diffuse disorder scattering. *Acta Crystallography*, *14*(11), 1180–1185.
Swatloski, R. P., Holbrey, J. D., Weston, J. L., & Rogers, R. D. (2006). Preparation of magnetic cellulose composites using ionic liquids. *Chemistry Today*, *24*, 31–35.
Swatloski, R. P., Spear, S. K., Holbrey, J. D., & Rogers, R. D. (2002). Dissolution of cellose with ionic liquids. *Journal of the American Chemical Society*, *124*, 4974–4975.
Vonk, C. G. (1973). Computerization of Ruland's X-ray method for determination of the crystallinity in polymers. *Journal of Applied Crystallography*, *6*, 148–152.
Wada, M., Kondo, T., & Okano, T. (2003). Thermally induced crystal transformation from cellulose Iα to Iβ. *Polymer Journal*, *35*, 155–159.
Wada, M., Nishiyama, Y., Chanzy, H., Forsyth, T., & Langan, P. (2008). *The structure of celluloses*. International Centre for Diffraction Data. ISSN 1097-0002.
Wang, H., Gurau, G., Kelley, S. P., Myerson, A. S., & Rogers, R. D. (2013). Hydrophobic vs. hydrophilic ionic liquid separations strategies in support of continuous pharmaceutical manufacturing. *RSC Advances*, *3*, 10019–10026.
Wang, H., Gurau, G., & Rogers, R. D. (2012). Ionic liquid processing of cellulose. *Chemical Society Reviews*, *41*, 1519–1537.
Wendler, F., Graneß, G., Büttner, R., Mechtler, K., & Heinze, T. (2006). A novel polymeric stablizing system for modified lyocell solutions. *Journal of Polymer Science, B: Polymer Physics*, *44*, 1702–1713.
Wendler, F., Graneß, G., & Heinze, T. (2005). Characterization of autocatalytic reactions in modified cellulose/NMMO solutions by thermal analysis and UV/VIS spectroscopy. *Cellulose*, *12*, 411–422.
Wendler, F., Meister, F., Wawro, D., Wesolowska, E., Ciechanska, D., Saake, B., et al. (2010). Polysaccharide blend fibres formed from NaOH, *N*-methylmorpholine-*N*-oxide and 1-ethyl-3-methylimidazolium acetate. *Fibres & Textiles in Eastern Europe*, *18*, 21–30.
Zhao, Y. L., Liu, X. M., Lu, X. M., Zhang, S. J., Wang, J. J., Wang, H., et al. (2012). The behavior of ionic liquids under high pressure: A molecular dynamics simulation. *Journal of Physical Chemistry B*, *116*, 10876–10884.
Zhu, S. D., Wu, Y. X., Chen, Q. M., Yu, Z. N., Wang, C. W., Jin, S. W., et al. (2006). Dissolution of cellulose with ionic liquids and its application: A mini-review. *Green Chemistry*, *8*, 325–327.